Voxel-based population analysis for correlating local dose and rectal toxicity in prostate cancer radiotherapy

Oscar Acosta [1,2], Gael Drean [1,2], Juan D. Ospina[1,2], Antoine Simon[1,2], Pascal Haigron[1,2], Caroline Lafond[1,2,3] and Renaud de Crevoisier[1,2,3]

[1] INSERM, U1099, Rennes, F-35000, France;

[2] Université de Rennes 1, LTSI, Rennes, F-35000, France;

[3]Département de Radiothérapie, Centre Eugène Marquis, Rennes, F-35000, France

E-mail: oscar.acosta@univ-rennes1.fr

Abstract. The majority of current models utilized for predicting toxicity in prostate cancer radiotherapy are based on dose-volume histograms. One of their main drawbacks is the lack of spatial accuracy, since they consider the organs as a whole volume and thus ignore the heterogeneous intra-organ radio-sensitivity. In this paper, we propose a dose-image-based framework to reveal the relationships between local dose and toxicity. In this approach, the three-dimensional (3D) planned dose distributions across a population are non-rigidly registered into a common coordinate system and compared at a voxel level, therefore enabling the identification of 3D anatomical patterns, which may be responsible for toxicity, at least to some extent. Additionally, different metrics were employed in order to assess the quality of the dose mapping. The value of this approach was demonstrated by prospectively analyzing rectal bleeding ($\geq$Grade 1 at 2 years) according to the CTCAE v3.0 classification in a series of 105 patients receiving 80Gy to the prostate by IMRT. Within the patients presenting bleeding, a significant dose excess (6Gy on average, $p<0.01$) was found in a region of the anterior rectal wall. This region, close to the prostate (1cm), represented less than 10% of the rectum. This promising voxel-wise approach allowed subregions to be defined within the organ that may be involved in toxicity and, as such, must be considered during the inverse IMRT planning step.

Keywords: Prostate cancer radiotherapy, rectal bleeding, toxicity prediction, spatial characterization, population analysis, non-rigid registration, predictive models

Submitted to: *Phys. Med. Biol.*

1. Introduction

Radiation therapy (RT) is a commonly used efficacious treatment for prostate cancer (PC). Several strategies have been developed in order to improve local control, particularly by increasing the radiation dose with highly conformal techniques, suggesting a strong dose-effect relationship (Zietman et al., 2010). Nowadays, the precision of treatment delivery is steadily improving due to the combination of intensity modulated RT (IMRT) and image-guided RT (IGRT). Hence the possibilities for achieving better control by increasing the dose are within reach. However, dose escalation is limited by rectal and urinary toxicity (Fonteyne et al., 2008; Fiorino, Rancati and Valdagni, 2009). Thus, the new competences of the delivery systems could be efficiently exploited following adapted planning provided that accurate predictive toxicity models are available. The understanding of dose-volume *versus* toxicity relationships, therefore, becomes crucial for selecting appropriate constraints at the inverse planning step in IMRT.

The prediction of complications resulting from the irradiation has been extensively treated in the literature (Fiorino, Rancati and Valdagni, 2009). These predictions are commonly based on the planned dose distribution via the dose-volume histograms (DVH) (Ting et al., 1997) using radiobiological normal tissue complication probability (NTCP) models (Jensen et al., 2010; Cambria et al., 2009; Grigorov et al., 2006; Wachter et al., 2001). In the case of prostate cancer RT, different studies have shown a reproducible correlation between dose, volume, and rectal toxicity (Benk et al., 1993; Fiorino et al., 2002; Sohn, Alber and Yan, 2007; Marzi et al., 2007; Rancati et al., 2004; Fiorino, Valdagni, Rancati and Sanguineti, 2009; Peeters et al., 2006). However, current DVH-based models for toxicity prediction exhibit several limitations. Firstly, they do not implicitly integrate the subject's individual specificities, such as medical history, or concomitant treatments, such as chemotherapy or androgen deprivation, in their formulation. Nevertheless, these patient-specific parameters may be considered by stratifying the population (Fiorino et al., 2008) at the expense of statistical power. Secondly, these models lack spatial accuracy, as they are not able to correlate the treatment outcome with the spatial dose distribution, thereby considering the organs as having homogeneous radio-sensitivity. Hence, the subtle potential correlation between local dose and toxicity may not be detected when the rich three-dimensional (3D) dose distribution is represented as a single organ DVH. The loss of local information may be aggravated when the DVH is further reduced to a single value such as the effective dose (D_{eff}) or equivalent uniform dose (EUD), which has also been shown to be correlated with the risk of toxicity (Schwarz et al., 2004; Rancati et al., 2004). Under these assumptions, depicting the relationship between local dose and toxicity is expected to be very informative, as it may be instrumental in identifying subregions at a higher risk of damage and thus facilitate the definition of more accurate dose-organ constraints.

The notion of spatial local dose variability and its relationship with toxicity have been already addressed in a limited number of works (Kupchak et al., 2008), either using a parametric description of the dose distribution (Buettner et al., 2009, 2011)or, for the first time, a voxel-based approach (Heemsbergen et al., 2010; Witte et al., 2010), although with

approximations in terms of both anatomical matching and dose mapping. In these two voxel-wise studies, which were focused on urinary tract toxicity (Heemsbergen et al., 2010)and prostate tumor control (Witte et al., 2010), the dose mapping was mainly based on the radially-computed distances from the organ delineations. These results provided the way forward for complex voxel-based toxicity models based on more accurate inter-individual matching. In order for voxel-wise comparisons to be meaningful, the doses must be accurately mapped to a common coordinate system, which is a challenging task due to the difficulties related to high inter-individual variability.

In response to the lack of spatial information of DVH-based predictive models, this paper proposes a new framework allowing the underlying relationship between local dose and toxicity to be analyzed across a population. This approach permits the identification of subregions within the critical organs, which may present a higher risk of damage and likely be responsible for toxicity. As depicted in Figure 1, the proposed framework combines a precise anatomical non-rigid registration approach for mapping the population 3D dose distributions to a single coordinate system and a voxel-wise analysis with respect to toxicity. The proposed model yields a 3D map $\Phi(x)$, $x \in \mathbb{R}^3$, which may be seen as a 3D NTCP cartography, depicting regions where the dose differences between two groups are statistically significant.

2. Materials and Methods

The main steps of the method are described in Figure 1: i) the inter-individual CT and contour delineations are non-rigidly registered (NRR) into a common coordinate system (common template) using organ-to-organ constraints; ii) the planned dose distributions are mapped to the template by applying the computed transformations (dense deformation field $\vec{D}$); iii) voxel-wise comparison of the mapped doses is performed (in this work, two-sampled t-tests for hypothesis testing). The resulting 3D images represent the dose differences between two groups and allow for the highlighting of voxels where those differences are statistically significant.

[Figure 1 HERE]

2.1. Patients, treatment and rectal toxicity

A total of 105 patients were included in the study, all having undergone IMRT for localized prostate cancer between July 2006 and June 2010 in the same institution. The target volume involved the prostate and seminal vesicles, without any lymph nodes. The total prescribed dose was 46Gy to the seminal vesicles delivered in 4.6 weeks, and 80Gy to the prostate delivered in 8 weeks, with a standard fractionation of 2Gy/fraction. The whole treatment (patient positioning, CT acquisition, and volume delineations) and dose constraints complied with GETUG 06 recommendations, as previously reported (Beckendorf et al., 2011). In particular, the constraints for the rectal wall were maximal dose $\leq$76Gy and V72 Gy$\leq$25%. The size of the planning CT images in the axial plane was 512x512 pixels, with 1mm image resolution, and 2mm slice thickness. The used treatment planning system was Pinnacle V7.4 (Philips Medical System, Madison, WI). Each treatment plan used five field beams, in a step-

and-shoot delivery configuration with gantry angles of 260°, 324 textdegree, 36°, 100°and 180°. The delivery was guided by means of an IGRT protocol, with cone beam CT images or two orthogonal images (kV or MV imaging devices), using gold fiducial markers in 57% of patients.

The median follow-up period was 38 months, with a minimum of 24 months for all patients. Rectal toxicity events were prospectively collected, as all of the patients participated in one of two randomized trials, either the GETUG 14 (testing the benefit of 4-month androgen deprivation in addition to receiving 80Gy of radiation to the prostate) or the STIC-IGRT (testing the benefit of IGRT) (De Crevoisier et al., 2009). Rectal toxicity was scored according to the common terminology criteria for adverse events (CTCAE) version 3.0. The endpoint of the study was 2-year Grade ≥ 1 rectal bleeding, excluding acute toxicity. Patients with a history of hemorrhoids were not allowed to be scored as Grade 1 bleeding. In total, 24 patients presented at least a Grade 1 rectal bleeding event, which occurred between 6 and 24 months following treatment.

2.2. Inter-individual registration and dose mapping

Three issues were addressed for mapping inter-individual 3D dose distributions to a single coordinate system: i) selection of the common coordinate system (template); ii) registration of the inter-individual anatomies; iii) propagation of the individual dose distributions to the template.

2.2.1. Template selection One question that arises when defining a common coordinate system for population analysis is the computation of inter-individual similarities (Aljabar et al., 2009; Wu et al., 2007; Commowick and Malandain, 2007). In order to diminish the bias inherent to using a single template, one potential strategy is to select a typical individual from the database, which is quite similar to the majority of individuals. Thus, intensity-based similarity metrics may define the distance between individuals (Aljabar et al., 2009). Given an adequate inter-individual similarity, the strategy may further include a clustering step aimed to identify the average individual that best represents the population (Ramus and Malandain, 2010).

In this study, a typical individual was selected from the database in order to define the template. This individual was found by affinity propagation clustering (Frey and Dueck, 2007)among a subgroup of randomly selected patients from the whole database. During the clustering step, the template emerged as the exemplar, which represented the individual closest to all of the remaining individuals. The considered inter-individual similarity criteria were the sum of squared differences (SSD) computed after rigid registration between individuals I_K and I_L

$$SSD = -\frac{1}{N}\sum_{x\in\Omega}|I_K(x) - I_L(x)|^2, \tag{1}$$

where N is the number of voxels x in the CT scans and Ω represents the pelvic region

where the computation was performed. Figure 2 shows the selected template with delineated organs representation.

[FIGURE 2 HERE]

2.2.2. Registration Registering inter-individual CTs is particularly challenging due to the poor soft-tissue contrast, large inter-individual variability, and differences in bladder and rectum filling (Acosta et al., 2011). Given this inter-individual anatomical matching, pure intensity-based registration was shown to be not accurate enough to meet the requirements for population analysis, possibly leading to non-negligible local errors (Drean et al., 2011). However, if all the complementary information pertaining to the individual's anatomy was used, the registration's performance would improve considerably. We propose herewith an organ-driven non-rigid registration strategy built from the demons algorithm (Thirion, 1998), which yields an accurate match between organs in the common coordinate system (CS). This non-rigid registration approach advantageously exploits information available at the planning stage, namely the 3D anatomical data, 3D organ delineations, and planned doses as summarized in Fig. 3 and detailed below.

Let I_k represent an individual to be registered in the template I_T: i) for each individual's delineated organ $O_k = \{Prostate_k, Bladder_k, Rectum_k\}$ an Euclidean distance map $L(O_k)$ (Danielsson, 1988) was first computed. Thus, each map $L_{O_k}(\mathbf{x})$ represented for each $\mathbf{x} \in \mathbb{R}^3$ within the organ, a distance to the O_k surface. Likewise for the counterpart in the template $O_T = \{Prostate_T, Bladder_T, Rectum_T\}$ and corresponding distance maps $L_{O_T}(\mathbf{x})$; ii) each of the distance maps was mutually normalized, yielding a set of normalized distance maps as $NL_{O_k}(\mathbf{x}) = max\{L_{O_T}(\mathbf{x})\} \cdot L_{O_k}(\mathbf{x})$ and $NL_{O_T}(\mathbf{x}) = max\{L_{O_k}(\mathbf{x})\} \cdot L_{O_T}(\mathbf{x})$. iii) The NL of both I_k and I_T were then superposed over the CT scans, replacing the original organ delineations; iv) the demons algorithm (Thirion, 1998) was finally used to non-rigidly register I_k to I_T. These NL_{O_k} constituted additional anatomic constraints, which facilitated the anatomic matching process. The use of Euclidean distance maps from organ surfaces reinforced accurate matching of doses close to the boundaries where pure intensity-based CT registration would fail. The result of this registration step was a dense deformation field $\vec{D}(x)$, which was then used to propagate the dose as shown in Fig. 4.

[FIGURE 3 HERE]

2.2.3. Dose propagation The deformation field $\vec{D}(x)$, obtained in the previous step, is a set of $3D$ vectors defined at each voxel (Fig.4), thereby providing a non-linear transformation to be applied to the dose distributions.

The doses were eventually propagated into the template by applying $\vec{D}(x)$ to each voxel position $\in I_k$ and sampled again in the space of I_T using tri-linear interpolation. Figure 5 shows an example of dose propagated from an individual towards the template.

[FIGURE 4 HERE]

2.3. Scores for validation of registration and dose mapping

Different parameters were used in order to assess the quality of the dose mapping. These parameters validated both the accuracy of organ overlap after non-rigid registration as well as the coincidence of doses between the native and common coordinate systems. Regarding registration, the Dice similarity coefficient (DSC) and Hausdorff distance (H) were used. The DSC (Zijdenbos et al., 1994) is defined as:

$$DSC = 2\left(\frac{R_T \cap R_I}{|R_T| + |R_I|}\right) \tag{2}$$

where $\cap$ is the intersection between each individual's registered rectum R_I and the rectum of the template R_T. This score ranges from 0 to 1 as a function of the volume overlap.

The Hausdorff distance (Hausdorff, 1918), implemented in (Commandeur et al., 2011)‡ was used in order to compute the distance H between two sets of points or surfaces $S_1 = \{s1_1, ..., s1_p\}$ and $S_2 = \{s2_1, ..., s2_q\} \in \mathbb{R}^3$ as:

$$H\left(S_1, S_2\right) = \max\left\{h\left(S_1, S_2\right), h\left(S_2, S_1\right)\right\} \tag{3}$$

where

$$h\left(S_1, S_2\right) = \max_{s1 \in S_1} \min_{s2 \in S_2} \parallel s1 - s2 \parallel \tag{4}$$

and $\parallel \cdot \parallel$ is the euclidean distance between the S_1 and S_2 points. The calculation $h\left(S_1, S_2\right)$ identifies the point $s1 \in S_1$ that is farthest from any point of S_2 and measures the distance from $s1$ to its nearest neighbor in S_2 using $\parallel \cdot \parallel$. This means that $h\left(S_1, S_2\right)$ ranks each point of S_1 based on its distance to the nearest point of S_2 , and then uses the largest ranked point as the distance (Huttenlocher et al., 1993).

For the validation of dose coincidence between native and common spaces, in order to compare dose mapping accuracy, we implemented two scores pertaining to the relative difference of areas (RDA) of DVHs and dose-organ overlap (DOO).

The RDA assesses the differences in DVHs following dose mapping while considering the information in the template coordinate system. For a given individual, let h_1 be the DVH computed between the mapped dose and the non-rigidly registered rectum, and let h_2 be the DVH computed with the warped dose and the rectum of the template,

$$RDA(h_1, h_2) = \frac{\int_0^{dose_{\max}} |h_1 - h_2|\, du}{\max\left\{\int_0^{dose_{\max}} h_1 du, \int_0^{dose_{\max}} h_2 du\right\}} \tag{5}$$

The RDA is normalized between 0 (when $h_1 = h_2$) and 1 using the area under the DVH curve. The DVHs are expected to be preserved following registration. Therefore, if RDA tends to zero, a DVH-based NTCP model would be similar, whether computed in the native space or the common coordinate systems.

‡ open source available at: http://www.vtkjournal.org/browse/publication/839

The DOO is a score that measures the coincidence of both the organs and dose distribution in the common space following registration. This parameter is computed as follows:

$$DOO\left(dose, R_I, R_T\right) = \frac{\int\limits_{R_I \cap R_T} dose\left(x\right) dx}{\int\limits_{R_I \cup R_T} dose\left(x\right) dx} \tag{6}$$

where $D(x)$ is the registered dose distributions at x, computed on the union and intersection of both organs (template and registered). The DOO penalizes the overlap errors within the higher gradients of dose. Conversely, if the overlap is measured in a region of homogeneous dose, the score is the same as the Jaccard similarity metric (JAC), namely:

$$JAC = \left(\frac{R_T \cap R_I}{R_T \bigcup R_I}\right) \tag{7}$$

where $\bigcup$ represents the union of both R_T and R_I. Hence, the DOO ranges between 0 and 1, attaining the highest value when the dose on each voxel of both organs is the same.

2.4. Voxel-based Analysis

Statistical voxel-based comparisons are instrumental in detecting regional changes between groups by locally computing the difference of a signal across a given population (Friston KJ et al., 1995). Different examples were reported in the literature, such as voxel-based morphometry (VBM) (Ashburner and Friston, 2000), which allow the differences related to density changes in a given tissue, such as gray matter changes in the brain on account of a disease, to be assessed (Yuan et al., 2008). These differences may reflect local anatomical changes, such as tensor-based morphometry (Hua et al., 2008; Leow et al., 2007), the analysis of which relies on Jacobian images obtained by warping individual data to a common template. Some studies have combined hypometabolism and atrophy using positron emission tomography (PET) images, where the differences may be accounted for by functional integrity (Chételat et al., 2008; Desgranges et al., 2007).

In our study, the signals to be compared on a voxel level were the 3D planned dose distributions across the population. Two groups were therefore constituted, namely individuals with rectal bleeding *versus* those with no rectal bleeding, according to the inclusion criteria described in section 2.1. In order for the voxel-wise comparisons to be meaningful, only accurately registered rectum data was included. Registration accuracy was measured as a high-volume overlap (Dice score >0.7) between the rectum in template space and NRR individuals. As a result, two groups were obtained, comprising 51 non-bleeding and 12 bleeding subjects, respectively. Voxel-wise two-sampled t-tests were performed, resulting in 3D maps for both dose differences and p-values. The regions exhibiting statistically significant between-group differences ($p < 0.01$) were characterized in terms of absolute volume, mean dose difference, and rectal localization in the rectum, more precisely distance of the region to the prostate and seminal vesicle surfaces.

3. Results

Fig. 5 depicts an example of the dose mapping from the individual's native coordinate system to the template coordinate system using the proposed framework.

Considering the whole population, the average dice score for the rectum was 0.75 ± 0.12 and the Hausdorff distance $28.17mm \pm 16$, while the DOO and the RDA were 0.64 ± 0.1 and 0.09 ± 0.05, respectively.

[FIGURE 5 HERE]

Figure 6 depicts the between-group dose differences in the rectum. The dose prescribed to patients with rectal bleeding was significantly higher (6.43Gy, p<0.01) in a small portion of the rectum (labeled R1). Figures 6(b) and 6(c) show lateral and coronal views of the 3D reconstructed common template highlighting the region R1. This 3184.06 mm^3 region, located in the anterior wall and middle-third of the rectum, represented 9.11% of the total rectal volume.

Table 1 characterizes the distribution of statistically significant voxels (region R1) with respect to the distance to the prostate and seminal vesicles surfaces. 35.86% of R1 was within the first 5mm, receiving in average 4.55 Gy more within the rectal bleeding patients but more than 90% of R1 was located within the first centimeter (anterior wall). This result shows that the more sensitive area was within the first 10 to 15mm, and that within this region, the average dose delivered to rectal bleeding patients was exceeded by +6.40Gy as compared to that delivered to non-bleeding patients.

Figure 7 shows the averaged DVHs within R1, compared with the DVHs computed for the whole rectum. Inside R1, the differences between bleeding and non-bleeding patients were between $V_{40}Gy$ and $V_{66}Gy$, reaching statistical significance ($p < 0.01$), as opposed to the whole rectum where no significant differences were found.

[FIGURE 6 HERE]

[TABLE 1 HERE]

[FIGURE 7 HERE]

4. Discussion

The particular novelty presented here, in comparison with traditional DVH-based models, makes maximal use of 3D dose distributions, resulting in a correlation between local toxicity and local planned dose. The proposed method relies on an accurate non-rigid registration strategy allowing the dose distributions across a population to be mapped and compared on a common coordinate system. The voxel-wise analysis would permit the identification of subregions within the organs at risk, which may be responsible for secondary effects, hence highlighting heterogeneous intra-organ radio-sensitivity.

The Grade $\geq$1 bleeding toxicity was chosen as the main endpoint in this study, as such events are relatively frequent when high-dose is delivered to the prostate (approximately 20% after 2 years) allowing for statistical tests to be performed. In addition, rectal bleeding is a symptom that can be relatively objectively reported (excluding patients with a history of

hemorrhoids). Moreover, most of the studies assessing NTCP models for rectal toxicity are focused on rectal bleeding.

Based on our results, the anterior part of the rectal wall correlated with rectal bleeding. This region, representing less than 10% of the whole rectum, was given 6Gy more, on average, in bleeding patients and was mainly located within the first 15mm, close to where high-dose was delivered to the prostate. In addition, the average DVH computed within this region allowed for better separation between both groups, resulting in a clear volume effect (Fig. 7).

These results are in line with the Lyman-Kutcher-Burman NTCP model studies, which reported effective volume values (often denoted by n) between 0.06 and 0.13 for moderate/severe bleeding, thus highlighting the high-dose range impact and suggesting that the rectum was a prevalently serial organ. Indeed, in our study, a small non circumferential volume within the anterior part of the rectum was found to be correlated with rectal bleeding (grade>=1). However, the "intermediate" doses inside this rectal region better discriminate bleeders from non-bleeders, as it is discussed in (Rancati et al., 2004). Nevertheless, results from the literature as well as from our voxel-based comparison study must be interpreted with caution, taking into account several RT parameters. These results depend on the ability of the conformal technique to spare the posterior part of the rectum from "intermediate" dose levels (40Gy to 50Gy), total dose prescribed in the prostate, and dose volume constraints in the rectum, potentially allowing a high-dose to be delivered to the anterior rectal wall. The observation that the anterior part of the rectum appears to be involved in rectal bleeding equally corresponds to the clinical experience of rectal cauterization. This finding is in line with a report on a series of 44 patients who voluntarily accepted to undergo flexible rectosigmoidoscopy. In this investigation, the occurrence of telangiectasia increased from the posterior to the anterior rectal wall, and Grade 3 telangiectasia was exclusively limited to the high-dose region of the anterior rectal wall (Wachter et al., 2000).

Nevertheless, it should be noted that the toxicity results must be carefully considered in terms of cause-effect relationships. We are depicting regions that are correlated with toxicity, which are not necessarily responsible for it. New cohorts of patients are required in order to validate the hypothesis raised by means of this voxel-based approach. New findings in terms of dose-toxicity relationships may appear for other symptoms. Larger series of patients would allow for a multivariate analysis to be performed, taking into account patient-specific characteristics in addition to the treatment parameters. Other organs should also be explored, such as the bladder, where most of the models have not found any dose-effect relationship.

Another key point to take into account is the potential difference between the planned and actual delivered doses. In effect, in the course of the treatment, the organs at risk may deform or displace with respect to the initial conditions at the planning step. This is also an issue for the current NTCP models that consider only planned dose distributions. In our study, however, more than half of the included patients were treated following an IGRT protocol, which likely minimizes the impact of anatomical variations, at least to some extent. The next generation of NTCP models should ideally be established on both planning imaging, as well as imaging acquired during each fraction. This issue is currently being tackled in further works, where dose-tracking strategies may help improve accuracy. In addition, statistical approaches are

being developed so as to model these uncertainties (Söhn et al., 2005), considering the actual delivered dose as a random variable, while investigating the impact of the deformations on toxicity outcome.

The proposed framework, as depicted in Figure 1, relies on a non-rigid matching of organs and CT scans. The use of Euclidean distance maps from organ boundaries allowed for accurate matching of doses close to the rectal wall. Additionally, further registration approaches are being investigated to improve the aligning of different structures. A combined CT-organ registration with a spatial weighted function was recently proposed (Drean et al., 2012), but still needs to be validated within this framework.

Another point to be investigated in future research is the optimal template selection. Different strategies exist to select a template from a database to be representative of a given population. In some applications, an average individual may be obtained by iteratively registering and computing intensity means (Rohlfing et al., 2004). Other approaches are based on group-wise registration (Wachinger and Navab, 2012). In our clustering strategy, we selected a single representative individual, however, more clusters may also be selected in order to reproduce the voxel-wise analysis on different templates (Rohlfing et al., 2009). The question brought to mind is therefore the computation of inter-individual similarities, which may be tackled, as already done in the past within the scope of atlas based segmentation (Rohlfing et al., 2004; Wu et al., 2007).

Concerning the voxel-based statistical dose analysis, we are considering other alternative approaches that take into account the effect of individuals, in line with the non-parametric mixed-effect model proposed by (Ospina et al., 2011, 2012). This method, which exploits intra-individual spatial correlation at each voxel location, can handle more efficiently large variances between groups. Preliminary results demonstrated an improved sensitivity and reliability for group analysis, as compared with standard voxel-wise methods. One interesting feature is the possibility of including clinical data or other confounding variables within the formulation. A similar method that is currently being explored is the dimensionality reduction of data (Chen et al., 2011) in order to extract the main spatial features of the 3D dose distributions, which would allow patients to be classified in two groups.

Determining the heterogeneous intra-organ sensitivity across a population, combined with patient-specific information in an inverse IMRT planning, may allow for the production of personalized treatment with high local control and reduced toxicity, as observed in other studies with different constraints (Söhn, Yan, Liang, Meldolesi, Vargas and Alber, 2007). This general scope may be extended in order to adapt ongoing treatment, thus taking into account not only data from a model but also integrating the dynamic individual specificities (i.e., tumor response and anatomical modifications). To achieve a more accurate prediction in inverse adaptive planning, further work should also consider the inclusion of the individual's clinical variables that may be involved in toxicity (age and concomitant treatments, etc.).

Within this perspective for adaptive radiotherapy, the set of parameters Φ extracted from the population data may be then combined with the individual's parameters $\phi_p(t)$, which may change during the treatment in order to better adapt the therapy. In practice, a comparison between equivalent treatment plans could be performed, allowing the best treatment *i.e.* the

treatment that spares the more sensitive regions, to be selected during therapy.

5. Conclusion

In this work, we have proposed a methodological framework based on non-rigid registration aimed at determining the local dose-effect relationship in prostate cancer radiotherapy, helping reveal the heterogeneous intra-organ radio-sensitivity to predict toxicity. It is based on a non-rigid registration scheme combining organ delineations with CT scans and thus enabling better organ matching among individuals. Our contribution exploits information available at the planning stage, namely the 3D anatomical data, 3D organ delineations, and planned doses. This study opens the door for new methods of analyzing toxicity with increased accuracy, which may eventually lead to improved constraints within IMRT planning.

References

Acosta, O., Simon, A., Monge, F., Commandeur, F., Bassirou, C., Cazoulat, G., de Crevoisier, R. and Haigron, P. (2011), Evaluation of multi-atlas-based segmentation of CT scans in prostate cancer radiotherapy, *in* 'Biomedical Imaging: From Nano to Macro, 2011 IEEE International Symposium on', pp. 1966 –1969.

Aljabar, P., Heckemann, R., Hammers, A., Hajnal, J. and Rueckert, D. (2009), 'Multi-atlas based segmentation of brain images: Atlas selection and its effect on accuracy', *Neuroimage* **46**(3), 726–738.

Ashburner, J. and Friston, K. (2000), 'Voxel-based morphometry–the methods', *Neuroimage* **11**(6 Pt 1), 805–821.

Beckendorf, V., Guerif, S., Prisé, E. L., Cosset, J.-M., Bougnoux, A., Chauvet, B., Salem, N., Chapet, O., Bourdain, S., Bachaud, J.-M., Maingon, P., Hannoun-Levi, J.-M., Malissard, L., Simon, J.-M., Pommier, P., Hay, M., Dubray, B., Lagrange, J.-L., Luporsi, E. and Bey, P. (2011), '70Gy versus 80Gy in localized prostate cancer: 5-year results of GETUG 06 randomized trial.', *Int J Radiat Oncol Biol Phys* **80**(4), 1056–1063.

Benk, V. A., Adams, J. A., Shipley, W. U., Urie, M. M., McManus, P. L., Efird, J. T., Willett, C. G. and Goitein, M. (1993), 'Late rectal bleeding following combined x-ray and proton high dose irradiation for patients with stages T3-T4 prostate carcinoma.', *Int J Radiat Oncol Biol Phys* **26**(3), 551–557.

Buettner, F., Gulliford, S. L., Webb, S. and Partridge, M. (2011), 'Modeling late rectal toxicities based on a parameterized representation of the 3D dose distribution', *Physics in Medicine and Biology* **56**(7), 2103.

Buettner, F., Gulliford, S. L., Webb, S., Sydes, M. R., Dearnaley, D. P. and Partridge, M. (2009), 'Assessing correlations between the spatial distribution of the dose to the rectal wall and late rectal toxicity after prostate radiotherapy: an analysis of data from the MRC RT01 trial (ISRCTN 47772397)', *Physics in Medicine and Biology* **54**(21), 6535.

Cambria, R., Jereczek-Fossa, B. A., Cattani, F., Garibaldi, C., Zerini, D., Fodor, C., Serafini, F., Pedroli, G. and Orecchia, R. (2009), 'Evaluation of late rectal toxicity after conformal radiotherapy for prostate cancer: a comparison between dose-volume constraints and NTCP use.', *Strahlenther Onkol* **185**(6), 384–389.

Chen, B., Acosta, O., Kachenoura, A., Ospina, J., Drèan, G., Simon, A., Bellanger, J.-J., Haigron, P. and de Crevoisier, R. (2011), Spatial characterization and classification of rectal bleeding in prostate cancer radiotherapy with a voxel-based principal components analysis model for 3d dose distribution, *in* A. Madabhushi, J. Dowling, H. Huisman and D. Barratt, eds, 'Prostate Cancer Imaging. Image Analysis and Image-Guided Interventions', Vol. 6963 of *Lecture Notes in Computer Science*, Springer Berlin / Heidelberg, pp. 60–69.

Chételat, G., Desgranges, B., Landeau, B., Mézenge, F., Poline, J. B., de la Sayette, V., Viader, F., Eustache, F. and Baron, J.-C. (2008), 'Direct voxel-based comparison between grey matter hypometabolism and atrophy in alzheimer's disease.', *Brain* **131**(Pt 1), 60–71.

Commandeur, F., Velut, J. and Acosta, O. (2011), 'A VTK algorithm for the computation of the Hausdorff distance', *VTK Journal-http://www.vtkjournal.org/browse/publication/839* (839).

Commowick, O. and Malandain, G. (2007), 'Efficient selection of the most similar image in a database for critical structures segmentation', *Medical Image Computing and Computer-Assisted Intervention–MICCAI 2007* pp. 203–210.

Danielsson, P-E., (1980), 'Euclidean Distance Mapping.', *Computer Graphics and Image Processing* **14**(3), 227–248.

de Crevoisier, R., Pommier, P., Bachaud, J., Crehange, G., Boutry, C., Chauvet, B., Nguyen, T., Laplanche, A., Aubelle, M. and Lagrange, J. (2009), 'Image-guided radiation therapy (IGRT) in prostate cancer: Preliminary results in prostate registration and acute toxicity of a randomized study', *International Journal of Radiation Oncology*Biology*Physics* **75**(3, Supplement), S99 –.

Desgranges, B., Matuszewski, V., Piolino, P., Chételat, G., Mézenge, F., Landeau, B., de la Sayette, V., Belliard, S. and Eustache, F. (2007), 'Anatomical and functional alterations in semantic dementia: a voxel-based MRI and PET study.', *Neurobiol Aging* **28**(12), 1904–1913.

Drean, G., Acosta, O., Simon, A., de Crevoisier, R. and Haigron, P. (2011), 'Evaluation of inter-individual pelvic CT-scans registration', *IRBM* **32**(5), 288–292.

Drean, G., Acosta, O., Simon, A., de Crevoisier, R. and Haigron, P. (2012), Inter-individual organ-driven CT registration for dose mapping in prostate cancer radiotherapy, *in* 'Biomedical Imaging (ISBI), 2012 9th IEEE International Symposium on', pp. 370 –373.

Fiorino, C., Cozzarini, C., Vavassori, V., Sanguineti, G., Bianchi, C., Cattaneo, G. M., Foppiano, F., Magli, A. and Piazzolla, A. (2002), 'Relationships between DVHs and late rectal bleeding after radiotherapy for prostate cancer: analysis of a large group of patients pooled from three institutions.', *Radiother Oncol* **64**(1), 1–12.

Fiorino, C., Fellin, G., Rancati, T., Vavassori, V., Bianchi, C., Borca, V. C., Girelli, G., Mapelli, M., Menegotti, L., Nava, S. and Valdagni, R. (2008), 'Clinical and dosimetric predictors of late rectal syndrome after 3d-crt for localized prostate cancer: preliminary results of a multicenter prospective study.', *Int J Radiat Oncol Biol Phys* **70**(4), 1130–1137.

Fiorino, C., Rancati, T. and Valdagni, R. (2009), 'Predictive models of toxicity in external radiotherapy: dosimetric issues.', *Cancer* **115**(13 Suppl), 3135–3140.

Fiorino, C., Valdagni, R., Rancati, T. and Sanguineti, G. (2009), 'Dose-volume effects for normal tissues in external radiotherapy: pelvis.', *Radiother Oncol* **93**(2), 153–167.

Fonteyne, V., Villeirs, G., Speleers, B., Neve, W. D., Wagter, C. D., Lumen, N. and Meerleer, G. D. (2008), 'Intensity-modulated radiotherapy as primary therapy for prostate cancer: report on acute toxicity after dose escalation with simultaneous integrated boost to intraprostatic lesion.', *Int J Radiat Oncol Biol Phys* **72**(3), 799–807.

Frey, B. J. and Dueck, D. (2007), 'Clustering by passing messages between data points', *Science* **315**, 972–976.

Friston KJ, Holmes AP, Worsley KJ, Poline JP, Frith CD, Frackowiak RSJ and Fr (1995), *Human Brain Mapping*, Wiley, chapter Statistical Parametric Maps in Functional Imaging: A General Linear Approach, pp. 189–210.

Grigorov, G. N., Chow, J. C. L., Grigorov, L., Jiang, R. and Barnett, R. B. (2006), 'IMRT: improvement in treatment planning efficiency using ntcp calculation independent of the dose-volume-histogram.', *Med Phys* **33**(5), 1250–1258.

Hausdorff, F. (1918), 'Dimension und äußeres maß', *Mathematische Annalen* **79**(1), 157–179.

Heemsbergen, W. D., Al-Mamgani, A., Witte, M. G., van Herk, M., Pos, F. J. and Lebesque, J. V. (2010), 'Urinary obstruction in prostate cancer patients from the dutch trial (68 gy vs. 78 gy): Relationships with local dose, acute effects, and baseline characteristics.', *Int J Radiat Oncol Biol Phys* .

Hua, X., Leow, A. D., Parikshak, N., Lee, S., Chiang, M.-C., Toga, A. W., Jack, C. R., Weiner, M. W., Thompson, P. M. and Initiative, A. D. N. (2008), 'Tensor-based morphometry as a neuroimaging biomarker for Alzheimer's disease: an MRI study of 676 AD, MCI, and normal subjects.', *Neuroimage* **43**(3), 458–469.

Huttenlocher, D. P., Klandermand, G. A. and Rucklidge, W. J. (1993), 'Comparing images using the hausdorff distance', *IEEE Transactions on Pattern Analysis and Machine Intelligence* **15**(9), 850–856.

Jensen, I., Carl, J., Lund, B., Larsen, E. H. and Nielsen, J. (2010), 'Radiobiological impact of reduced margins and treatment technique for prostate cancer in terms of tumor control probability (TCP) and normal tissue complication probability (NTCP).', *Med Dosim* .

Kupchak, C., Battista, J. and Dyk, J. V. (2008), 'Experience-driven dose-volume histogram maps of NTCP risk as an aid for radiation treatment plan selection and optimization.', *Med Phys* **35**(1), 333–343.

Leow, A., Yanovsky, I., Chiang, M.-C., Lee, A., Klunder, A., Lu, A., Becker, J., Davis, S., Toga, A. and Thompson, P. (2007), 'Statistical properties of jacobian maps and the

realization of unbiased large-deformation nonlinear image registration', *Medical Imaging, IEEE Transactions on* **26**(6), 822 –832.

Marzi, S., Arcangeli, G., Saracino, B., Petrongari, M. G., Bruzzaniti, V., Iaccarino, G., Landoni, V., Soriani, A. and Benassi, M. (2007), 'Relationships between rectal wall dose-volume constraints and radiobiologic indices of toxicity for patients with prostate cancer.', *Int J Radiat Oncol Biol Phys* **68**(1), 41–49.

Ospina, J., Acosta, O., Drèan, G., Cazoulat, G., Simon, A., Correa, J., Haigron, P. and de Crevoisier, R. (2011), Spatial nonparametric mixed-effects model with spatial-varying coefficients for analysis of populations, *in* K. Suzuki, F. Wang, D. Shen and P. Yan, eds, 'Machine Learning in Medical Imaging', Vol. 7009 of *Lecture Notes in Computer Science*, Springer Berlin / Heidelberg, pp. 142–150.

Ospina, J., Benquet, P., Correa, J. and Acosta, O. (2012), A mixed effects spatio temporal model to assess the joint effect of ageing and alzheimer's disease in gray matter volume, *in* 'MICCAI-NIBAD 12 Workshop on Novel Imaging Biomarkers for Alzheimer's Disease and Related Disorders'.

Peeters, S. T. H., Hoogeman, M. S., Heemsbergen, W. D., Hart, A. A. M., Koper, P. C. M. and Lebesque, J. V. (2006), 'Rectal bleeding, fecal incontinence, and high stool frequency after conformal radiotherapy for prostate cancer: normal tissue complication probability modeling.', *Int J Radiat Oncol Biol Phys* **66**(1), 11–19.

Ramus, L. and Malandain, G. (2010), Assessing selection methods in the context of multi-atlas based segmentation, *in* 'Biomedical Imaging: From Nano to Macro, 2010 IEEE International Symposium on', IEEE, pp. 1321–1324.

Rancati, T., Fiorino, C., Gagliardi, G., Cattaneo, G. M., Sanguineti, G., Borca, V. C., Cozzarini, C., Fellin, G., Foppiano, F., Girelli, G., Menegotti, L., Piazzolla, A., Vavassori, V. and Valdagni, R. (2004), 'Fitting late rectal bleeding data using different ntcp models: results from an italian multi-centric study (airopros0101).', *Radiother Oncol* **73**(1), 21–32.

Rohlfing, T., Brandt, R., Menzel, R. and Maurer, C. R. (2004), 'Evaluation of atlas selection strategies for atlas-based image segmentation with application to confocal microscopy images of bee brains.', *Neuroimage* **21**(4), 1428–1442.

Rohlfing, T., Sullivan, E. V. and Pfefferbaum, A. (2009), 'Subject-matched templates for spatial normalization.', *Med Image Comput Comput Assist Interv* **12**(Pt 2), 224–231.

Schwarz, M., Lebesque, J. V., Mijnheer, B. J. and Damen, E. M. F. (2004), 'Sensitivity of treatment plan optimisation for prostate cancer using the equivalent uniform dose (EUD) with respect to the rectal wall volume parameter.', *Radiother Oncol* **73**(2), 209–218.

Sohn, M., Alber, M. and Yan, D. (2007), 'Principal component analysis-based pattern analysis of dose-volume histograms and influence on rectal toxicity.', *Int J Radiat Oncol Biol Phys* **69**(1), 230–239.

Söhn, M., Birkner, M., Yan, D. and Alber, M. (2005), 'Modelling individual geometric variation based on dominant eigenmodes of organ deformation: implementation and evaluation.', *Phys Med Biol* **50**(24), 5893–5908.

Söhn, M., Yan, D., Liang, J., Meldolesi, E., Vargas, C. and Alber, M. (2007), 'Incidence of late rectal bleeding in high-dose conformal radiotherapy of prostate cancer using equivalent uniform dose-based and dose-volume-based normal tissue complication probability models.', *Int J Radiat Oncol Biol Phys* **67**(4), 1066–1073.

Thirion, J.-P. (1998), 'Image matching as a diffusion process: an analogy with maxwell's demons', *Medical Image Analysis* **2**(3), 243 – 260.

Ting, J. Y., Wu, X., Fiedler, J. A., Yang, C., Watzich, M. L. and Markoe, A. (1997), 'Dose-volume histograms for bladder and rectum.', *Int J Radiat Oncol Biol Phys* **38**(5), 1105–1111.

Wachinger, C. and Navab, N. (2012), 'Simultaneous registration of multiple images: Similarity metrics and efficient optimization', *IEEE Transactions on Pattern Analysis and Machine Intelligence* **In press**.

Wachter, S., Gerstner, N., Goldner, G., Pötzi, R., Wambersie, A. and Pötter, R. (2000), 'Endoscopic scoring of late rectal mucosal damage after conformal radiotherapy for prostatic carcinoma.', *Radiother Oncol* **54**(1), 11–19.

Wachter, S., Gerstner, N., Goldner, G., Pötzi, R., Wambersie, A. and Pötter, R. (2001), 'Rectal sequelae after conformal radiotherapy of prostate cancer: dose-volume histograms as predictive factors.', *Radiother Oncol* **59**(1), 65–70.

Witte, M. G., Heemsbergen, W. D., Bohoslavsky, R., Pos, F. J., Al-Mamgani, A., Lebesque, J. V. and van Herk, M. (2010), 'Relating dose outside the prostate with freedom from failure in the dutch trial 68 gy vs. 78 gy.', *Int J Radiat Oncol Biol Phys* **77**(1), 131–138.

Wu, M., Rosano, C., Lopez-Garcia, P., Carter, C. S. and Aizenstein, H. J. (2007), 'Optimum template selection for atlas-based segmentation.', *Neuroimage* **34**(4), 1612–1618.

Yuan, Q., Zou, L. and Chen, Q. (2008), '[voxel-based morphometric study of brain structure in alzheimer's disease].', *Sichuan Da Xue Xue Bao Yi Xue Ban* **39**(3), 496–499.

Zietman, A. L., Bae, K., Slater, J. D., Shipley, W. U., Efstathiou, J. A., Coen, J. J., Bush, D. A., Lunt, M., Spiegel, D. Y., Skowronski, R., Jabola, B. R. and Rossi, C. J. (2010), 'Randomized trial comparing conventional-dose with high-dose conformal radiation therapy in early-stage adenocarcinoma of the prostate: long-term results from proton radiation oncology group/american college of radiology 95-09.', *J Clin Oncol* **28**(7), 1106–1111.

Zijdenbos, A. P., Dawant, B. M., Margolin, R. A. and Palmer, A. C. (1994), 'Morphometric analysis of white matter lesions in MR images: method and validation', *Medical Imaging, IEEE Transactions on* **13**(4), 716–724.

6. Figures

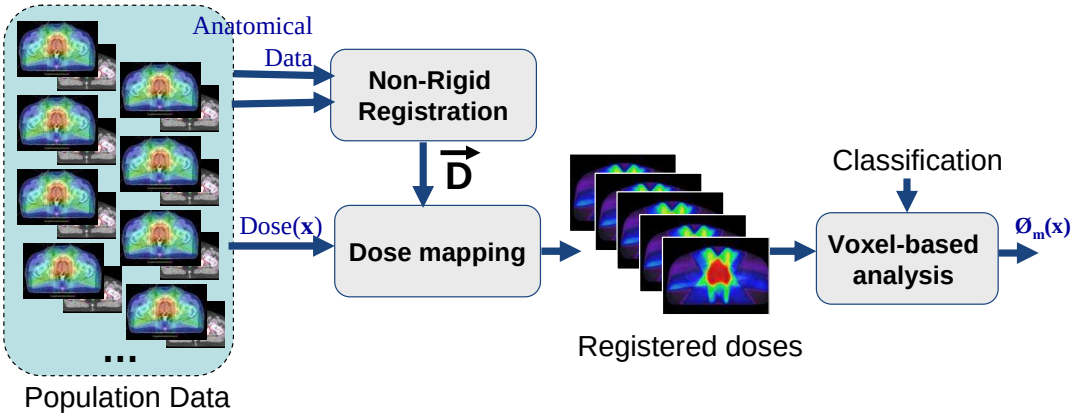

Figure 1. General framework of the proposed dose mapping and voxel-wise analysis. The anatomical information from a patient is NRR registered to a common template. The result is a vector field $\vec{D}$, which is used later on for dose mapping

.

(a) (b) (c)

Figure 2. Selected template. Sagittal views of the a) original CT scan, b) the organ delineations, and c) 3D representation. The prostate, rectum, bladder, and seminal vesicles (SV) are visible.

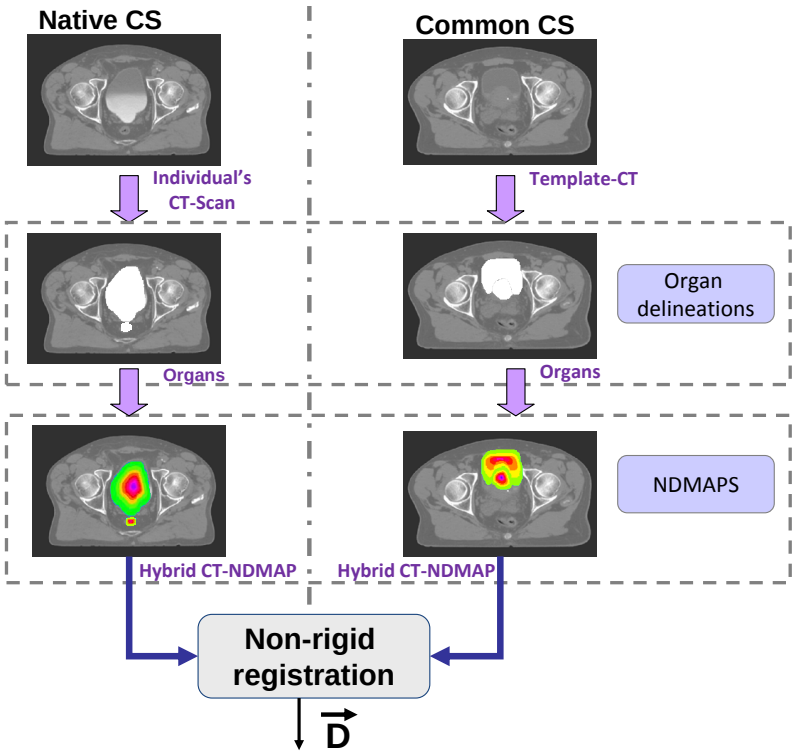

Figure 3. The hybrid non-rigid registration (NRR) approach, bringing 3D doses from their native coordinate system (CS) to the common CS. After organ delineation, normalized distance maps (NDMAPS) are computed and combined with the CT scan to be registered. The result is the transformation (deformation field) used to map the dose

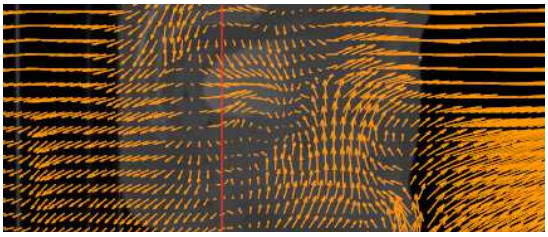

Figure 4. Example of the resulting transformation (deformation field, D) used to map the dose

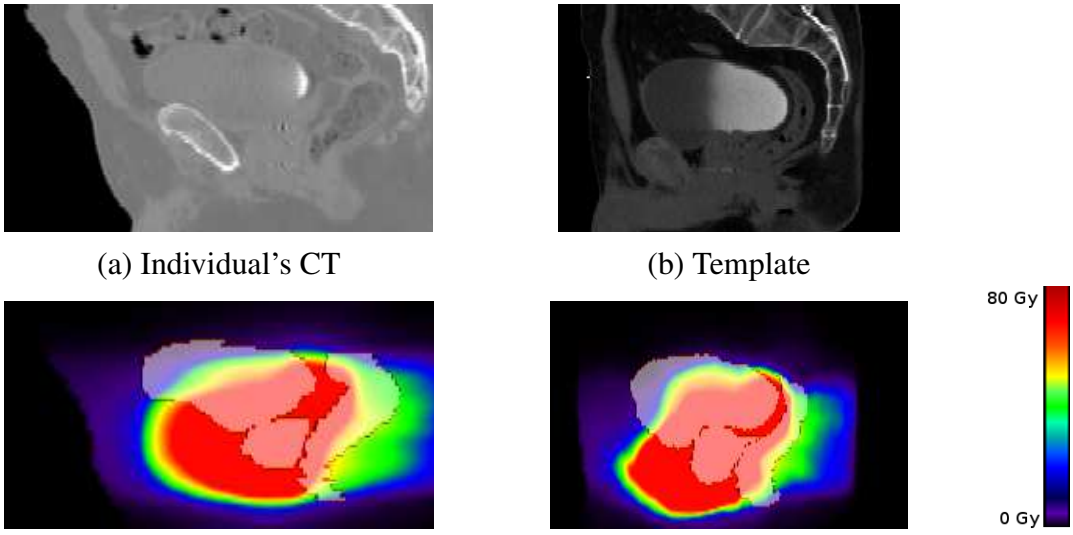

(a) Individual's CT (b) Template

(c) Individual's dose in the native space (d) Propagated dose to the template

Figure 5. Example of 3D non-rigid dose mapping using the computed transformation from Fig. 4. (a) A typical individual's CT; (b) the template; (c) an individual's TPS planned dose in the native coordinate system; (d) dose mapped to the template coordinate system

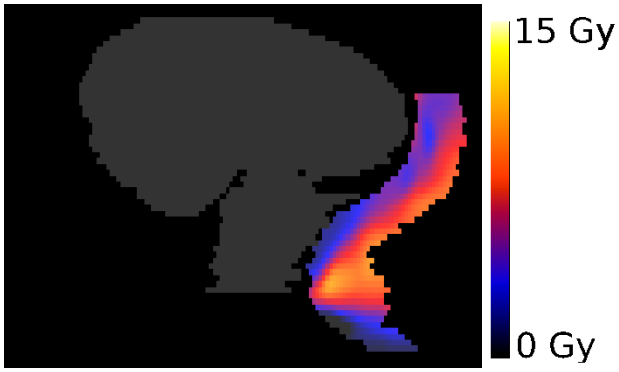

(a)

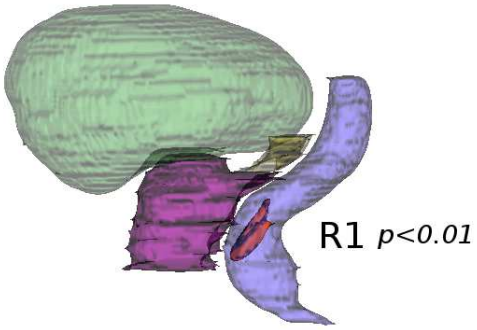

(b)

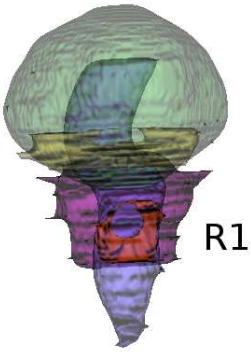

(c)

Figure 6. Results of voxel-wise analysis in the template space for rectal bleeding. a) Mean differences in dose between the two groups. b, c) 3-dimensional reconstruction of a) lateral and b) coronal views of the common template, highlighting the rectal region R1, where these differences were statistically significant ($p< 0.01$). In our study, this region represented less than 10% of the whole rectum and appears close to the prostate in the anterior rectal wall

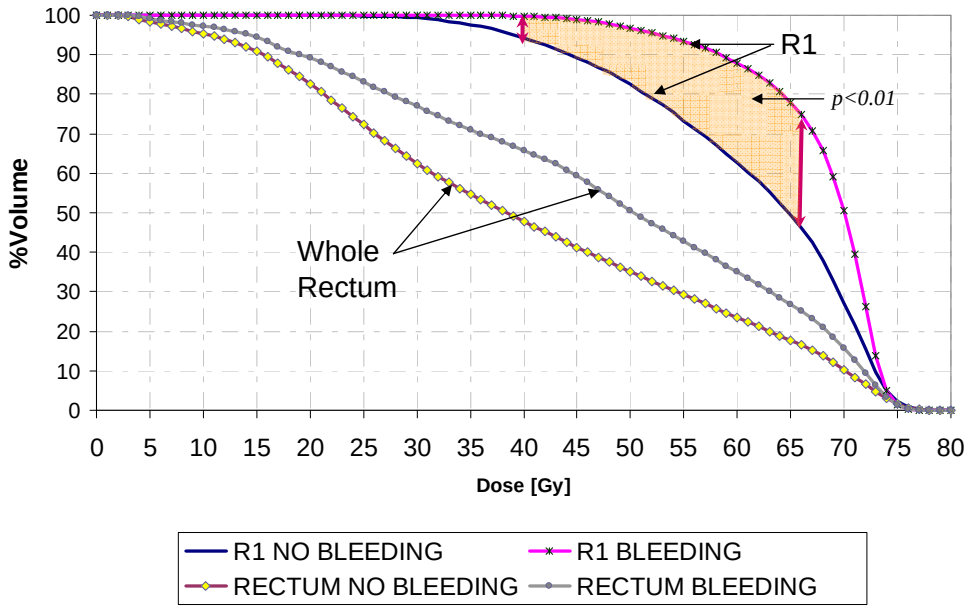

Figure 7. Averaged dose-volume histogram comparison for the two groups. They were computed in the rectum and in R1. The DVH for R1 allowed for the segmentation of a sub-region within the rectum, which correlated with rectal bleeding. In addition, the DVHs in R1 were significantly different ($p - values < 0.01$) for R1 between V_{40} and V_{66}

Table 1. Characterization of the statistically significant voxels ($p < 0.01$), R1, with respect to the distance to the prostate-seminal vesicle (PSV) surface: % of the whole significant region (R1) and mean dose difference

Rectal distance from PSV surface	**% of R1**	**Averaged dose difference**
5mm	35.86	4.55Gy
10mm	97.28	6.32Gy
15mm	98.97	6.43Gy
20mm	98.97	6.43Gy
30mm	98.97	6.43Gy